Electronic Supplementary Information

High Li^+ Transference Gel Interface between Solid-Oxide Electrolyte and Cathode for Quasi-Solid Lithium-Ion Batteries

Ramesh Subramani,[a] Yu-Hsien Tseng,[a] Yuh-Lang Lee,[a,b] Chi-Cheng Chiu,[a,b] Sheng-Shu Hou,[a,b] and Hsisheng Teng[a,b,c,*]

[a]Department of Chemical Engineering, National Cheng Kung University, Tainan 70101, Taiwan
[b]Hierarchical Green-Energy Materials (Hi-GEM) Research Center, National Cheng Kung University, Tainan 70101, Taiwan
[c]Center of Applied Nanomedicine, National Cheng Kung University, Tainan 70101, Taiwan
*E-mail: hteng@mail.ncku.edu.tw

Supporting information for:

1. Surface morphology of garnet LLZTO pellet

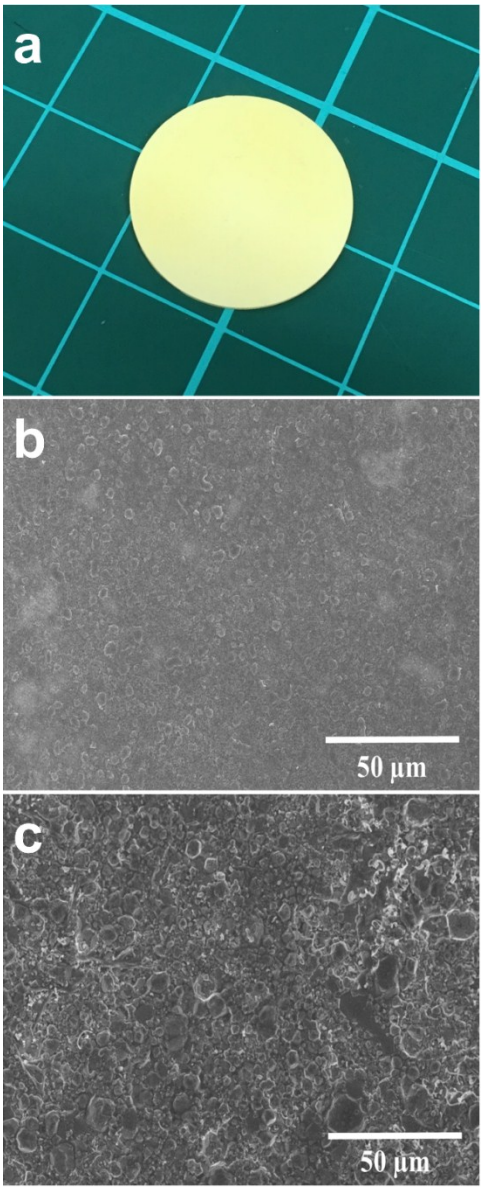

Fig. S1 Characteristics of the garnet LLZTO pellet. (a) Photograph of the finely polished garnet LLZTO pellet. (b,c) SEM images of the LLZTO pellet, (b) top view and (c) cross-sectional view.

2. Morphology of P(AN-co-MA) membrane and GPE

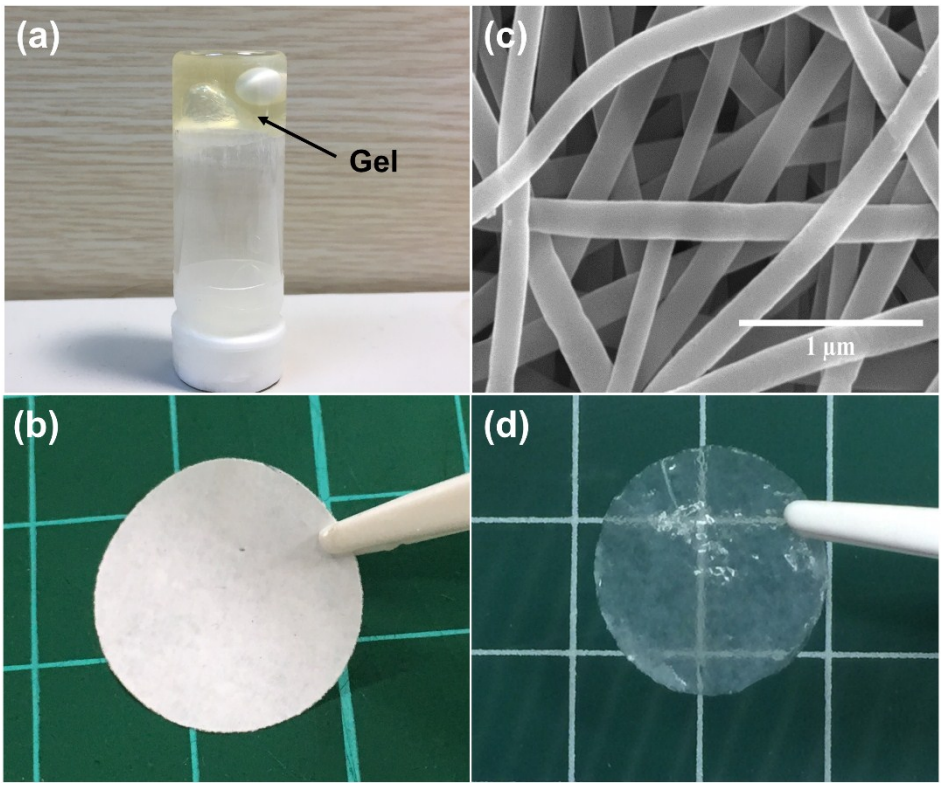

Fig. S2 Morphology of the P(AN-co-MA) membrane and GPE. (a) Mixture of the LE and P(AN-co-MA) at a mass ratio of 20:1. (b) Photograph of the P(AN-co-MA) membrane. (c) SEM image of the P(AN-co-MA) membrane. (d) Photograph of the GPE membrane.

3. Ionic conductivity of GPE and LE

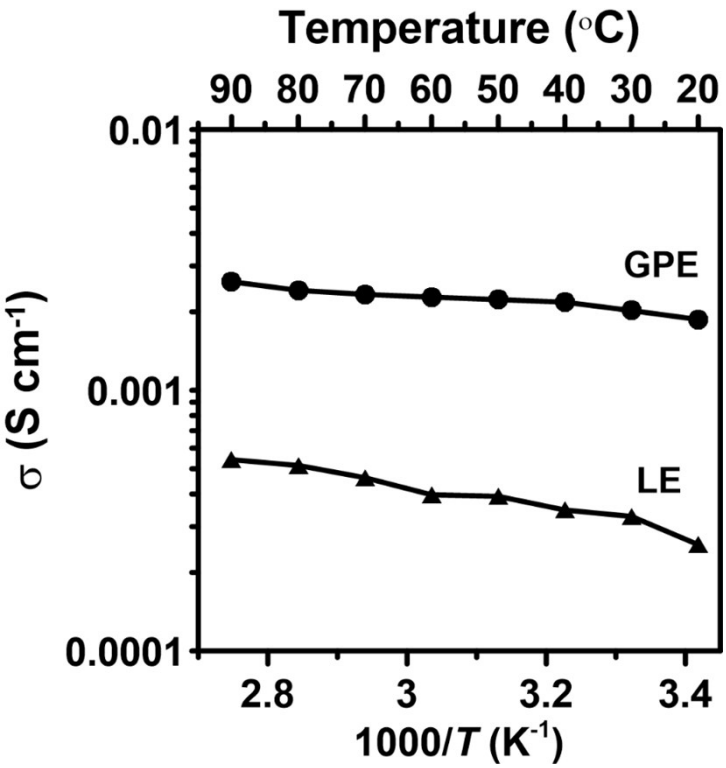

Fig. S3 Temperature dependence of the ionic conductivity of the GPE and separator-supported LE presented in an Arrhenius plot. The electrolytes was sandwiched between two stainless-steel electrodes for the measurements in a temperature range of 20–90 °C.

4. Determination of electrolyte t_{Li+} values

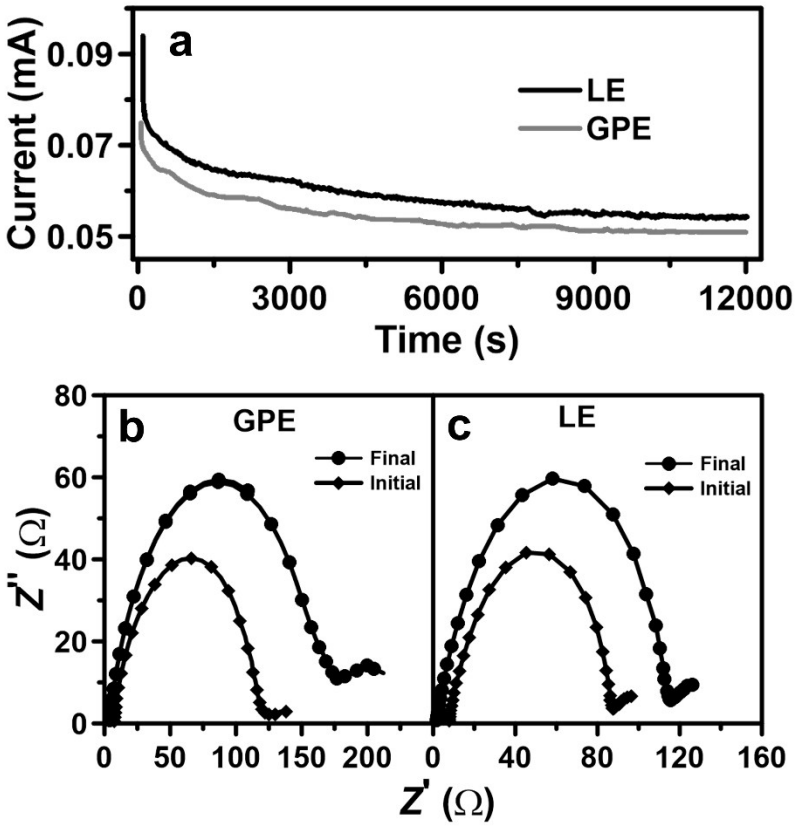

Fig. S4 (a) Current−time curves of the Li|electrolyte|Li cells following application of a DC voltage of 10 mV to the cells. (b,c) Corresponding Nyquist impedance plots of the cells using electrolytes (b) GPE and (c) separator-supported LE. The impedance plots were used to determine the initial ($R_{int,0}$) and final ($R_{int,ss}$) resistance values.

5. Stable voltage range of electrolytes

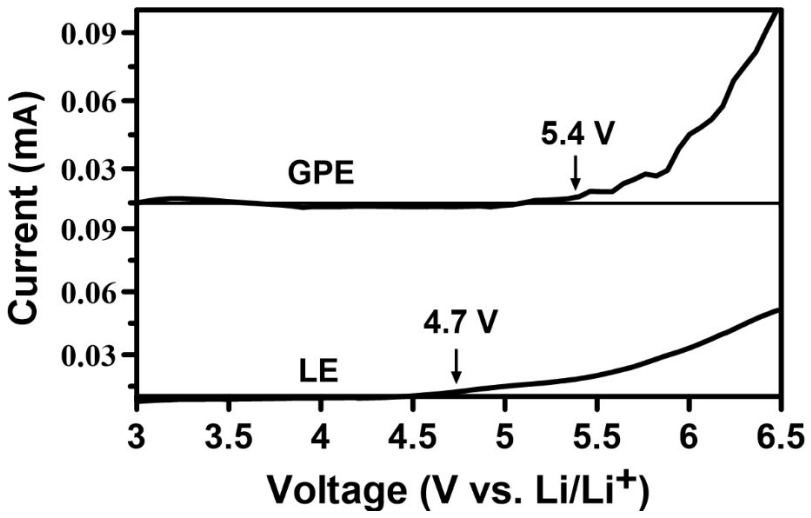

Fig. S5 Linear scan voltammetry curves for the GPE and separator-supported LE with a scan rate of 5 mV s^{-1}. Li-metal and stainless-steel electrodes were used as the reference and working electrodes, respectively.

6. Current dependence of battery discharge capacities

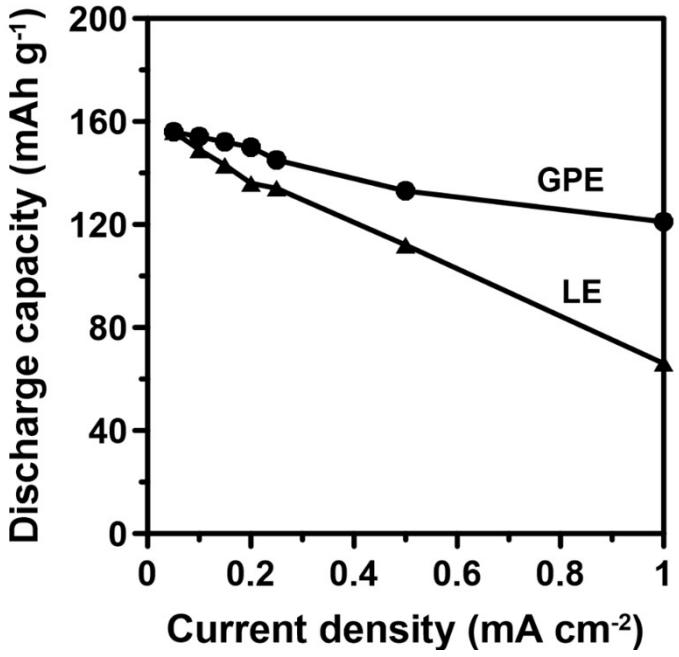

Fig. S6 Variation in discharge capacity with discharge current densities (0.05−1 mA cm^{-2}) for the Li|(Al/LLZTO/interlayer)|$LiFePO_4$ batteries with interlayers of the GPE and LE.

7. Cycling performance of Li|(Al/LLZTO/LE)|$LiFePO_4$

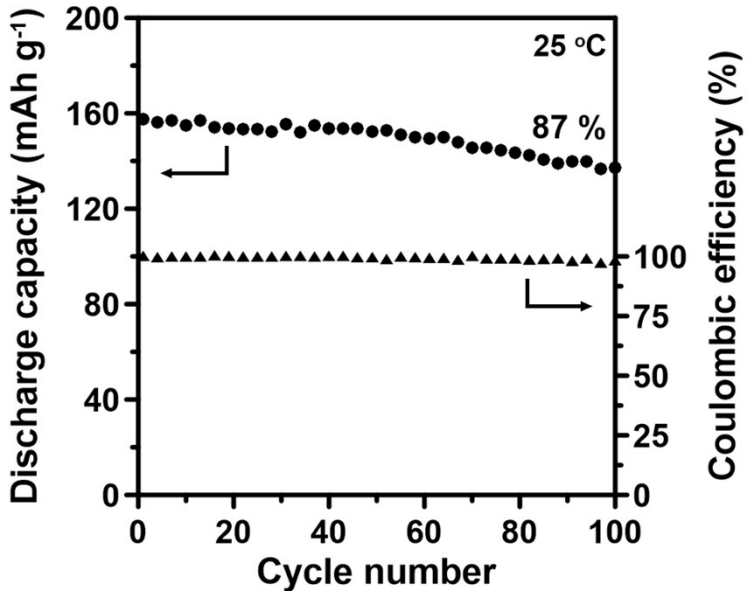

Fig. S7 Galvanostatic charge–discharge cycling performance of the Li|(Al/LLZTO/LE)|$LiFePO_4$ battery at 0.05 mA cm^{-2}.

8. Rate capability test for Li|(Al/LLZTO/GPE)|$LiFePO_4$

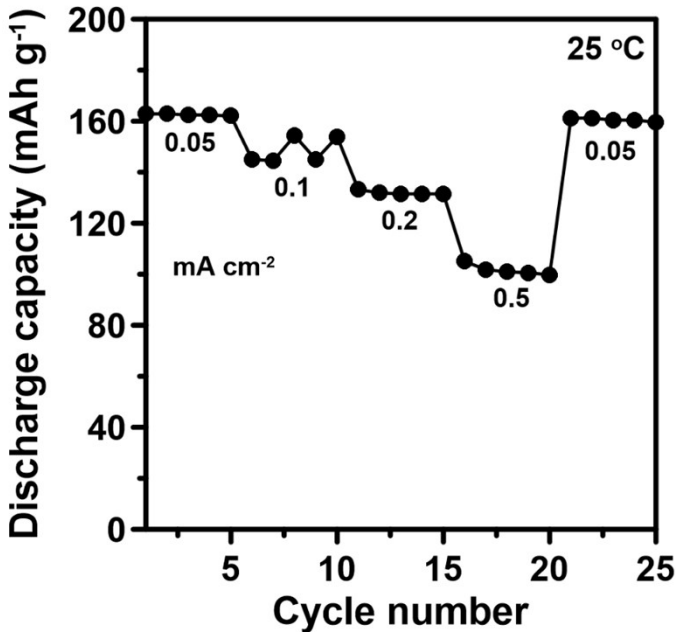

Fig. S8 Room-temperature (25 °C) discharge capacities of the Li|(Al/LLZTO/GPE)|$LiFePO_4$ battery in a series of galvanostatic charge−discharge cycles at various current densities**.**

9. Impedance spectra of the batteries

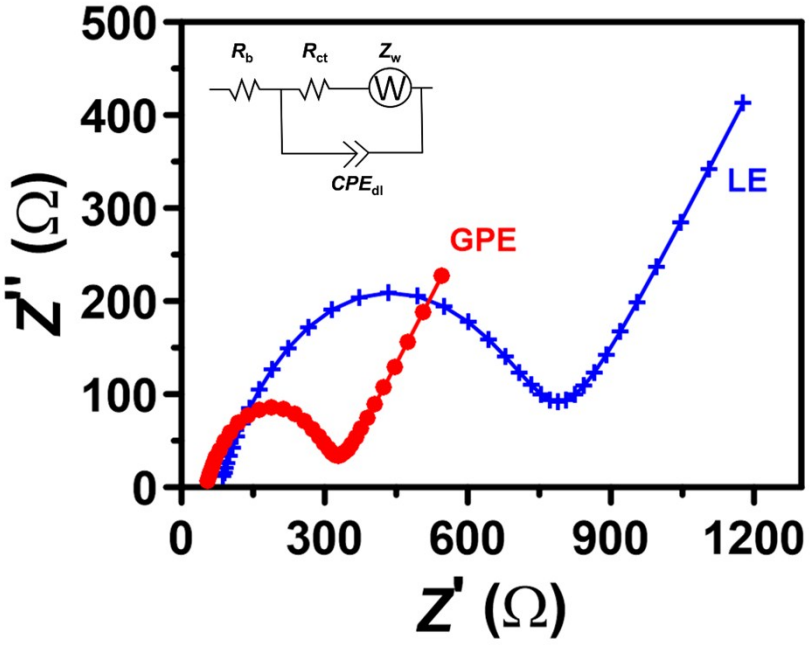

Fig. S9 Impedance spectra of the batteries Li|(Al/LLZTO/GPE)|$LiFePO_4$ and Li|(Al/LLZTO/LE)|$LiFePO_4$ obtained at 3.4 V. The solid-line curves are the simulations of the impedance data based on the equivalent circuit presented as the figure inset.

10. Performance of Li|(GPE/LLZTO/GPE)|$LiFePO_4$

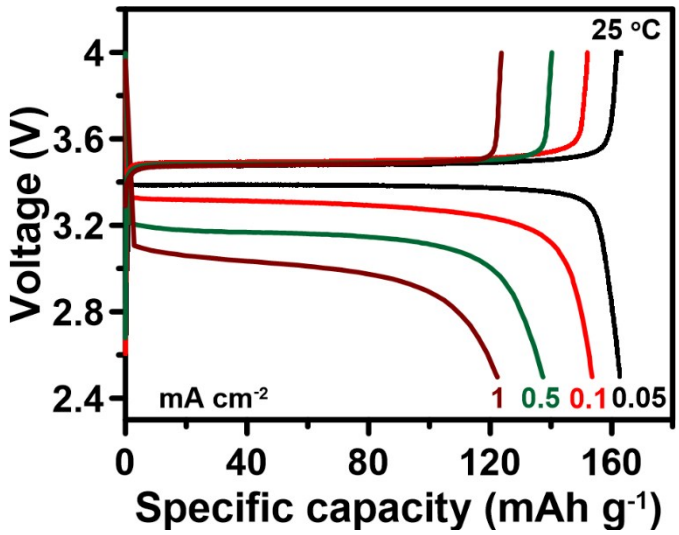

Fig. S10 Room-temperature (25 °C) galvanostatic charge–discharge profiles of the Li|(GPE/LLZTO/GPE)|$LiFePO_4$ battery operated at different discharge densities with the charge densities maintained at 0.05 mA cm^{-2}.